X-920-75-308

PREPRINT

NASA TM X- 71069

GRAVITY ANOMALY DETECTION — APOLLO/SOYUZ

F. O. VONBUN
W. D. KAHN
J. W. BRYAN
P. E. SCHMID
W. T. WELLS
T. D. CONRAD

DECEMBER 1975

GSFC — GODDARD SPACE FLIGHT CENTER —
GREENBELT, MARYLAND

CONTENTS

		Page
	ABSTRACT	v
	INTRODUCTION	1
I.	MATHEMATICAL METHODS	1
II.	PRELIMINARY RESULTS	6
III.	CONCLUSIONS	8
IV.	REFERENCES	9

ABSTRACT

The Goddard Apollo-Soyuz Geodynamics Experiment was performed to demonstrate the feasibility of tracking and recovering high frequency components of the earth's gravity field by utilizing a synchronous orbiting tracking station such as ATS-6. It was in reality the culmination of an effort started at Goddard in 1967/68 to utilize synchronous orbiting tracking stations for NASA missions. (Vonbun and Mengel 1967). Gravity anomalies of say 5 MGLS or larger having wavelengths of 300 to 1000 kilometers on the earth's surface are important for geologic studies of the upper layers of the earth's crust. Using a low orbiting (~ 230 km) spacecraft, such as Apollo-Soyuz continuously tracked by a synchronous satellite such as ATS-6, has for the first time detected from space short wavelength Earth's gravity anomalies (Vonbun 1971). Two prime areas of data collection have been selected for this particular experiment. One area is the center of the African continent and the second area is the Indian Ocean Depression centered at 5° north latitude and 75° east longitude.

Preliminary results show that the detectability objective of the experiment has been met in both areas as well as at several additional anomalous areas around the globe. Gravity anomalies of the Karakoram and Himalayan mountain ranges, ocean trenches, as well as the Diamantina Depth, could "be seen" to quote some specific examples. Further analyses are planned to demonstrate the utilization of the range rate signatures for the actual recovery of gravitational anomalies and their distribution on the earth's surface.

INTRODUCTION

The objectives of the Apollo/Soyuz Geodynamics Experiment were:

(a) To demonstrate the detectability of short wavelength (i.e. 300 km and larger) features of the Earth's gravity field,

(b) To evaluate the "High/Low" satellite to satellite tracking (SST) concept for geodynamics applications

and

(c) To test the recoverability of short wavelength features of the earth's gravity field.

The Apollo-Soyuz flying in a low orbit as mentioned, is particularly sensitive to gravity anomalies. For example, the ratio of sensitivity to the 25th degree terms of the earth's gravity potential having a wavelength of say 1600 kilometers is approximately 13 to 1 when going from a GEOS-3 type orbit (840 km) to the lower (230 km) Apollo orbit. Thus this mission gave us an excellent opportunity, which we could fortunately fully exploit, to test the satellite-to-satellite tracking concept.

Normal satellite perturbation methods used in the past for the computation of the earth's gravity field cannot be used for such short wavelengths because this would require a spherical harmonic expansion to an order and degree 120 or larger.

I. MATHEMATICAL METHODS

In general, the earth's gravitational field is in most cases represented in terms of a finite spherical harmonic series expansion whose coefficients have been determined from a combination of satellite ground tracking data and surface gravimetric data. As is known, such a limited representation of the global geopotential does not adequately "model" local variations in the gravity field. The reason being is that these local variations are too small in wavelengths and therefore would require a field expansion to a very high degree an order, i.e., in the order of 100 to 200 which seems impractical if not impossible. On the other hand, rather small local gravity anomalies are important for geologic investigations of the upper crust as well as for studies of the ocean topography (Vonbun 1975). The experiment as described and executed gives us an opportunity to improve our knowledge of the Earth's gravitational field in localized areas by "directly"

measuring local gravity variations by detecting small velocity changes of the low orbiting spacecraft. "Small" in this sense means 1 to 10 millimeters per second. Before going into some details on the gravity anomaly analyses some basics about the tracking system will be presented. Figure 1 shows the schematic of the ATS-6/ Apollo links. As can be seen, the Apollo is connected with Madrid via two links, namely, the ATS-6 link and a direct ground link. This provides a total loop as far as the measurements are concerned which will be used in the future to reduce the errors in the system but will not be discussed in this particular report. Here we shall concentrate only on the link Madrid-ATS-6-Apollo and back. Figure 2 depicts those quantities which are actually measured during the experiment. The system is constructed in such a fashion to measure the total range rate between the ground station, in this case Madrid, and the Apollo spacecraft in earth orbit. The total range rate is the sum of the range rates between Madrid-ATS ($\dot{r}_1$), ATS-Apollo ($\dot{r}_2$), Apollo-ATS ($\dot{r}_3$) and ATS-Madrid ($\dot{r}_4$) (Schmid, Vonbun 1974). For our analysis we will, however, only concentrate on the range rate variations between Apollo and ATS that is $\dot{\rho}_A$ which is just a dot product of the spacecraft velocity vector and the unit vector between Apollo and ATS as seen in Figure 2.

$$\dot{\rho}_A = (\vec{\rho}^0 \cdot \vec{v}) \tag{1}$$

One of the first tasks during the experiment was to evaluate the noise characteristics of the total system. Analysis done prior to the experiment predicted a range rate noise level of approximately 0.05 cm/sec utilizing a 10 second integration time depicted in Figure 3. This figure further shows that the actual experimental range noise level was lower than the predicted one is in the order of 0.03 cm/sec. These values were obtained using a small portion of an orbit so that possible orbit modelling errors where minimized. It should further be noted that these noise values are rather consistent through all the experimental arcs that have been analyzed.

In this paper, two approaches have been taken to test the detectability of gravity anomalies. The first one was to assume a single mass anomaly and to compute in a simple analytical fashion, the expected variation of the spacecraft velocity due to this anomaly, (Vonbun 1972). The velocity variations in the radial and horizontal components are then:

$$\Delta v_\rho = -\frac{\Delta m}{m} v_{hor} \left[\frac{1+x}{2(1-x)^2} \frac{\Delta\theta}{\sqrt{1 + \frac{x}{(1-x)^2}\Delta\theta^2}} + \frac{1}{2\sqrt{x}} \ln\left(\frac{\sqrt{x}}{1-x}\Delta\theta + \sqrt{1 + \frac{x}{(1-x)^2}\Delta\theta^2} \right) \right]$$

$$\Delta v_\theta = V_{horiz} \frac{\Delta m}{m} \left[\frac{1}{\sqrt{1 + x^2 - 2x\cos\Delta\theta}} - 1 \right] \qquad (2)$$

where

$$x = \left(\frac{R-d}{R+H} \right)$$

$$\Delta\theta = v \cdot t, \quad t \doteq 0 \text{ to } 150 \text{ sec}$$

R≡Radius of Earth, H≡Orbital Height in Kilometers, d≡Depth of Gravity Anomaly

see Fig. 4.

The above equations assume that the spacecraft travels directly over the anomaly and are only valid up to ±5° in true anomaly which corresponds to about 1.5 minutes of flight time. The dashed curve on Figure 4 shows the radial velocity variation due to a 5 mgal anomaly (4° by 4°). The size of the anomaly block was roughly twice the orbital height and represents the area of sensitivity of a spacecraft in orbit to an anomaly on the ground, (Schwartz 1970). Because of the extreme low noise in the data and the real geometry (spacecraft is not directly over the extended mass rather than point mass), a computer simulation was necessary to improve on the above shown analytical results.

The dotted line in Figure 4 depicts the result of this computerized analysis, which will now be briefly described. As shown in Figure 2 and mentioned earlier, the value $\dot{\rho}$ is equal (Bryan 1974):

$$\dot{\rho} = \dot{r}_1 + \dot{r}_2 + \dot{r}_3 + \dot{r}_4 \qquad (3)$$

this is the range rate as actually measured at the Madrid ATSR station. We are, however, only interested in the range rate between the Apollo spacecraft and the ATS spacecraft. That is:

$$\dot{\rho}_A = (\vec{v} \cdot \vec{\rho}_A^{\,0}) \qquad (4)$$

which is the dot product of the spacecraft orbital velocity vector $\vec{v}$ and the unit vector $\vec{\rho}^0$ between Apollo and ATS-6. Since the ATS-6 orbit is almost independent of any gravity variations because of its extreme height (36,000 km) its range rate can simply be subtracted from the measured one. That is

$$\dot{\rho}_A \doteq \dot{\rho} - \dot{\rho}\,(\text{ATS} - \text{Madrid}) \tag{5}$$

which brings us to one quantity needed for our further analyses. This range rate is on the other hand a function of

$$\dot{\rho}_A = f(X_A, X_{ATS}, G) \tag{6}$$

where X_A and X_{ATS} are Apollo and ATS-6 state vectors respectively and G represents the gravity field. The major aim in this experiment was to find the relationship between surface gravity anomalies Δg and the Apollo/ATS-6 range rate variations $\Delta\dot{\rho}_A$. To be more specific, we are interested only in the variation in $\dot{\rho}_A$, thus we want to vary equation (6).

$$\Delta\dot{\rho}_A \approx \frac{\partial f}{\partial X_A} \cdot \frac{\partial X_A}{\partial X_A^0} \Delta X_A^0 + \frac{\partial f}{\partial X_{ATS}} \cdot \frac{\partial X_{ATS}}{\partial X_{ATS}^0} \Delta X_{ATS}^0$$

$$+ \frac{\partial f}{\partial X_A} \left(\frac{\partial X_A}{\partial G} \right) \Delta G \tag{7}$$

and also:

$$\Delta\dot{\rho}_A = \left[(\Delta\vec{v}_\theta + \Delta\vec{v}_\rho) \cdot \vec{\rho}^0 \right] \doteq \text{(observed-computed) Range Rate}$$

The sensitivity coefficient $(\partial X_A / \partial G)$ is now contained in the equation 7 together with ΔG. Relating the actual measurements with the gravity potential variation ΔG. Since we are observing local anomalies over very short time only as can be seen in Figure 2 say in the order of a few minutes the first two terms on the right side of the series expansion can be neglected thus equation 7 reduces to

$$\Delta\dot{\rho}_A \approx \frac{\partial f}{\partial X_A} \cdot \left(\frac{\partial X_A}{\partial G} \right) \Delta G. \tag{8}$$

This sensitivity coefficient can now be computed utilizing Newton's equation of planetary motion:

$$\ddot{X}_A = f(X_A, G) \tag{9}$$

Differentiating (9) with respect to G yields:

$$\frac{\partial \ddot{X}_A}{\partial G} = \frac{\partial f}{\partial X_A} \frac{\partial X_A}{\partial G} + \frac{\partial f}{\partial G} \tag{10}$$

Since $(\partial X_A / \partial G)$ is our variable to be determined we rewrite equation (10) in the following manner assuming interchangeability of differential operators; that is:

$$\left(\frac{\partial \ddot{X}_A}{\partial G}\right) = \frac{d^2}{dt^2}\left(\frac{\partial X_A}{\partial G}\right) = \frac{\partial}{\partial X_A}\left(\frac{\partial V}{\partial X_A}\right) \cdot \frac{\partial X_A}{\partial G} + \frac{\partial}{\partial G}\left(\frac{\partial V}{\partial X_A}\right) \tag{11}$$

Where $V = U + T$ and U represents the normal potential of the earth's gravity field in spherical harmonics and

$$T = \frac{R}{4\pi} \iint_{\sigma} \Delta g S(\psi)\, d\sigma$$

Where $\Delta g = \Delta G + \Delta g_{LOC}$ using Δg_{LOC} as the local average anomaly of a block (say $4^\circ \times 4^\circ$ as an example), T is the disturbing potential due to the anomalies Δg, R is the radius of a sphere whose volume is equal to the volume of the spheroid and $S(\psi)$ the Stokes Function.

Introducing U and T into (11) yields finally:

$$-\frac{d^2}{dt^2}\left(\frac{\partial X_A}{\partial G}\right) = 2\,\frac{\partial^2}{\partial X_A^2}(U + T)\,\frac{\partial X_A}{\partial G} + \frac{\partial^2}{\partial X_A \partial G}(U + T) \tag{12}$$

Equation (12) is now solved for the sensitivity coefficient $(\partial X_A / \partial G)$ by numerical integration. Using equation (8), the above computed sensitivity coefficient is correlated and the relationship between $\Delta \dot{\rho}_A$ and ΔG established. In actuality the following procedures were used in detecting the gravity anomalies.

An orbit of 1 to 1.5 revolutions was computed for the Apollo spacecraft utilizing the (Preliminary Goddard Solution) PGS-108 gravity field using all tracking available, that is ground station as well as SST tracking data. From these Apollo orbits together with the ATS-6 orbit, the range rate $\dot{\rho}_A$ between ATS-6 and Apollo were computed. These range rate data were subtracted from the actual measured ones resulting in the $\Delta \dot{\rho}_A$ as shown in Figures 6 and 8. The reason that these values of $\Delta \dot{\rho}_A$ are finite rather than zero is the fact that we do not know the

gravity field to a very high accuracy which would necessarily include all the gravity anomalies. This is of course the essence of this particular experiment.

II. PRELIMINARY RESULTS

Experimental data were collected in the Eastern hemispheric region where the Apollo-Soyuz was in range of the ATS-6 satellite which is positioned over the equator at approximately 35° east longitude to perform the Indian Communications Experiment. The duration of each Apollo orbit, visible to ATS, was approximately 50 minutes or slightly greater than one half of an orbital revolution. The actual SST data passes used were only about 40 minutes long in order to assure non-disturbance of these data due to the earth's atmosphere. All data were successfully collected using the ATS-6 spacecraft and the Madrid ATS-R station as the prime ground station. Preliminary results confirm that the range rate noise of 0.05 cm/s computed before the experiment was exceeded by the experimental data which show an average noise of approximately 0.03 cm/sec (Fig. 3). Figure 5 shows the ground track of revolution 115 of the Apollo which coincidentally passes over two anomalies in the African area, as indicated. The gravity variations shown resulted from differencing two Goddard Earth Models (GEM-7 and GEM-8). The even GEM are constructed by using ground and satellite data where the odd numbered models are constructed only from satellite data. This difference thus reflects in essence the surface gravity anomalies though somewhat filtered by the models. These two anomalies have a variation of about ±5 mgals. In Figure 6 are depicted the theoretical variations of a 5 mgal anomaly (center) and superimposed (lower part) resulting in a total characteristic signature one would expect. In addition, the figure on the right also depicts the observed radial velocity variations. As can be seen, a fairly good agreement exists between the simulated and observed variations of the radial component of the spacecraft velocity except for a time delay. The dashed line shows finally the time shifted simulated variation of $\Delta\dot{\rho}_A$.

For this analysis the PGS 108 Field of order and degree of 25 was used. In that particular case the gravity anomalies are in the order of 5 mgals and extending over 300 to 2000 km were actually observed since the wavelength of the gravity anomaly and the resolution of this field are roughly compatible. This shows the usefulness of satellite-to-satellite tracking data to resolve anomalies of say ±5 mgals on the Earth's surface.

The second test area, namely the Indian Ocean Depression, is shown in Figure 7 in some detail utilizing again the Goddard Earth Model, Gem 6, but augmented

with 1° by 1° surface gravity data .n Figure 8, four orbital passes, namely 8, 23, 83, and 113, are plotted in the upper part of the graph. These orbits pass as can be seen over the Indian Ocean Depression as well as over the Himalayan Mountain range. The lower portion depicts the actual measurement residuals obtained, that is, the observed minus computed values. Both, the Indian Ocean Depression and anomalies in the Himalayan area can easily be "seen" in the actual data. Taking the Indian Depression as an example, the shape of the range rate variations do actually fit the expected one computed in a similar fashion as those shown in Figure 6. Detectability of the gravity field perturbations have thus been demonstrated, manifesting themselves in the expected form of small spacecraft velocity variations. The peak values of these variations could in most cases be closely correlated with anomalies shown on the detailed map of the global geoid. Other features may have been detected but cannot be verified at this time since there is a lack of surface gravimetric data in these areas. This is particularly true for the southern portion of the globe. One may however assume that the detected "gravity signatures" in the southern part of the earth represent existing anomalies not presently known too well.

Orbit determination required for the proper analysis of the experimental data to date involves the use of the satellite-to-satellite range rate data together with the direct ATS-6 tracking and the Unified S-Band tracking data. Error analysis performed (indicates that one and two revolution arcs seem to be the best in order to minimize the effects of unmodelled error in the detection and the recovery of gravity anomalies. Longer arcs seem to introduce larger errors because the influence of the Earth's gravity field errors onto the orbit errors become more and more pronounced as the arc length increases. Shorter arcs however have also rather large errors since not enough tracking data are available. Thus, the use of one to two orbit revolutions for the analyses seems to be a good optimum. Air drag corrections have been applied for the orbit determination of the Apollo-Soyuz. The satellite-to-satellite tracking data were only used during those periods which were judged free of on-board propulsion activities. Since the antenna is about 3 meters separated from the spacecraft axis any attitude motion (correction) of the spacecraft, that is a rotation of the spacecraft, transforms itself into a range rate between the Apollo-Soyuz and the ATS-6. One could therefore quite wrongly interpret a spacecraft rotation as a gravity anomaly on the ground. Detailed analysis of attitude control has not been performed at this time. Attitude data are, however, available and will be used in the future to further refine the range rate residuals as measured between Apollo-Soyuz and ATS-6.

CONCLUSION

Based upon the foregoing, it can be stated that the "high-low" satellite-to-satellite tracking technique can be utilized for earth gravity anomaly detection. Anomalies whose dimensions are equal or longer than the height of the low spacecraft and have values in the order of 5 mgals have been detected with a good 10:1 signal to noise ratio. The range rate of 0.05 cm/s conservatively computed prior to the experiment was actually exceeded by the measured noise of 0.03 cm/s. It was possible for all the passes checked so far, that the measured range rate residuals could be correlated with known geoidal features of short wave length of say 300 km or larger. It was further demonstrated that the range rate signatures could be repeated orbit by orbit thus increasing the confidence in the experimental data.

REFERENCES

Vonbun, F. O., Mengel, J. T., "Long Range Planning for Tracking and Communications for Manned Planetary Missions, AIAA, 4th Ann. Metg, Annaheim, Ca.lf., Oct. 1967, Journ. of Spacecraft and Rockets, Vol. 5, No. 7, July 68, pp. 863-865.

Vonbun, F. O., "The ATS-6/Nimbus 6 Satellite to Satellite Tracking Experiment," Rotation of the Earth, Symp. #46, Marioka, Japan, May 1971, D. Reider Publ. Comp., Dordrecht, Holland, 1972, pp. 112 to 120.

Vonbun, et al., "Sea Surface Determination from Space," GSFC Rept. X-900-75-216, Aug. 75 to be published in Journ. and Rockets.

Schwartz, E. R., "Gravity Field Refinement by Satellite to Satellite Doppler Tracking." Ph.D. Thesis, Ohio St. Univ. Rept. #147, Dec. 1970, NASA-Grant NGL-36-008-093.

Schmid, P., and Vonbun, F. O., "The ATS-F/Nimbus Tracking and Orbit Determination Experiment," IEEE, Intercon, N.Y., N.Y., Nov. 1974.

Bryan, J., "The ATS-F/GEOS C Satellite to Satellite Tracking Data Processing Considerations," GSFC Rept. #982-74-145, May 1974.

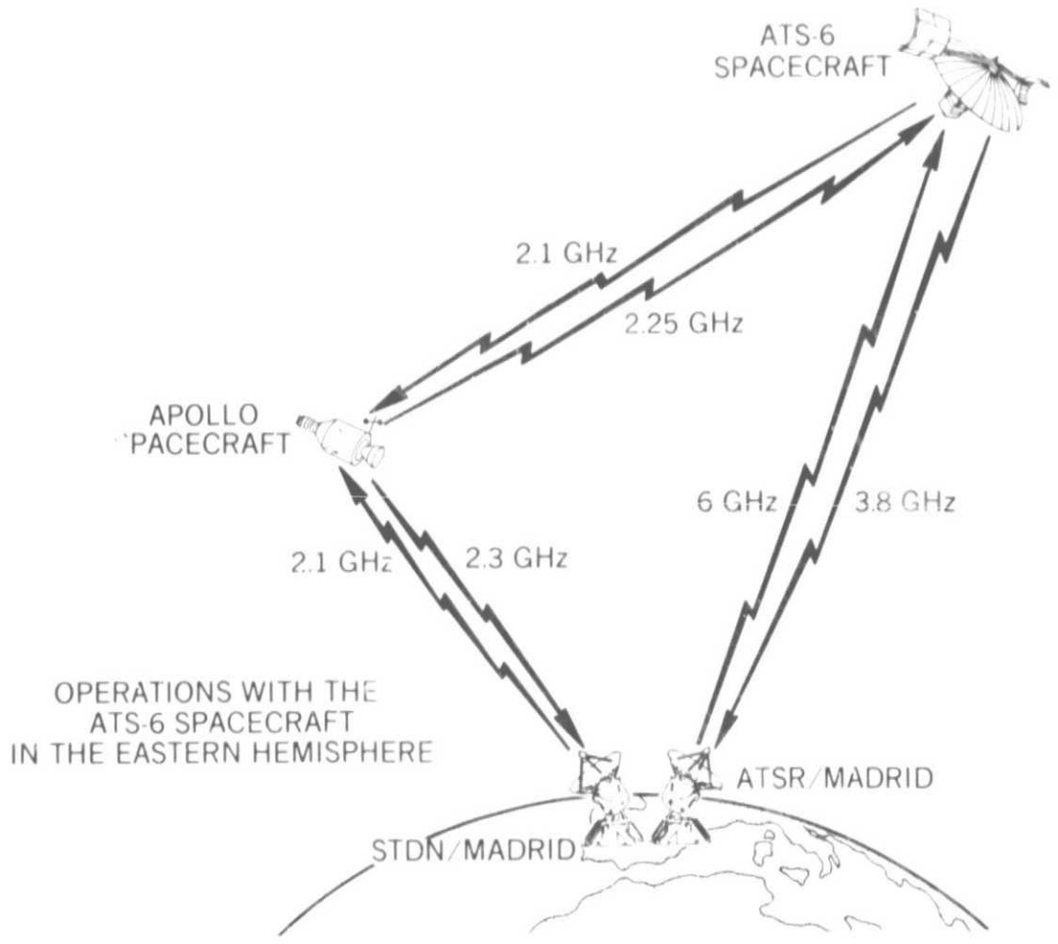

Figure 1. ATS-6/ASTP Geodynamics Experiment

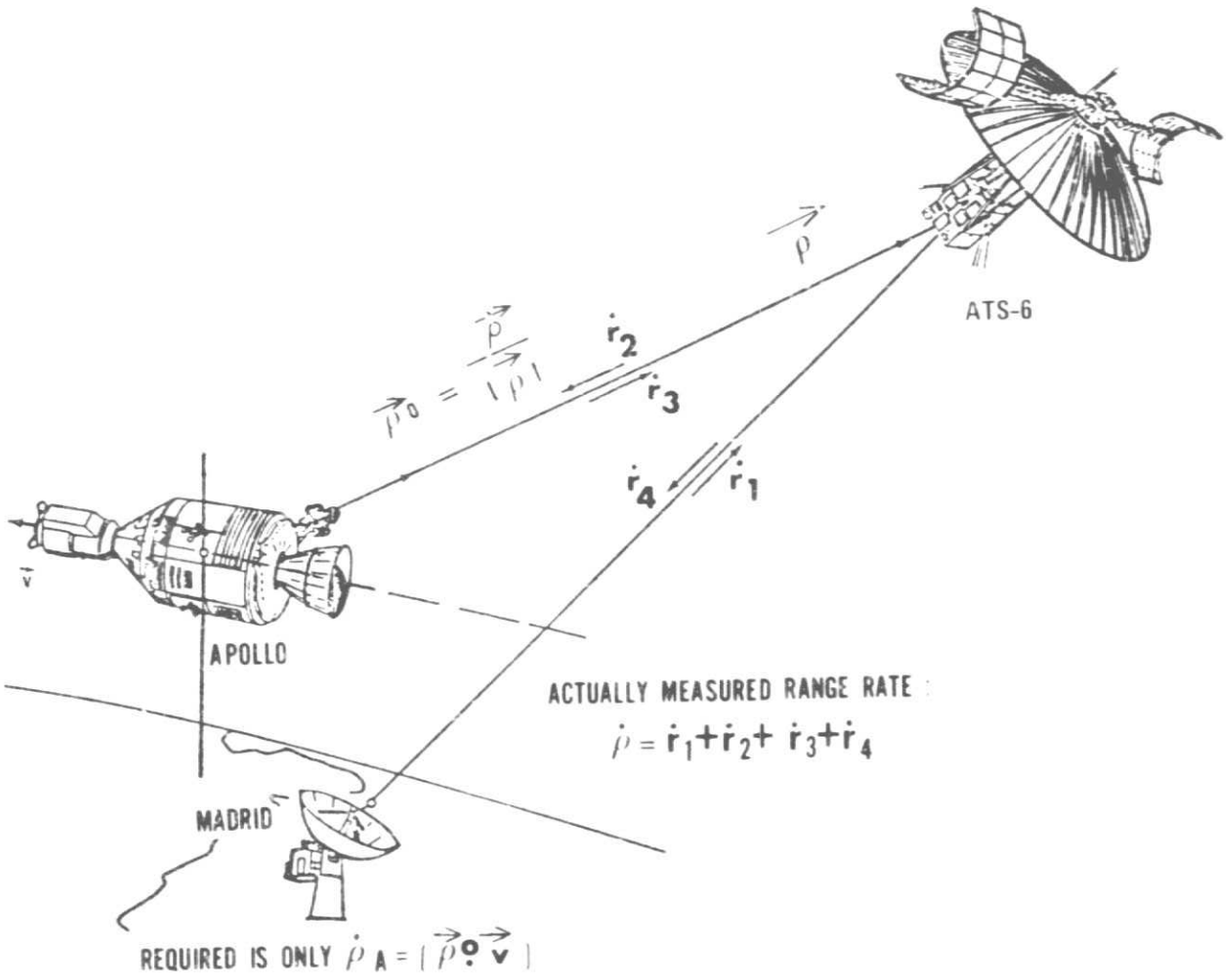

Figure 2. Range Rate Measurement Schematic for ATS-6 and Apollo

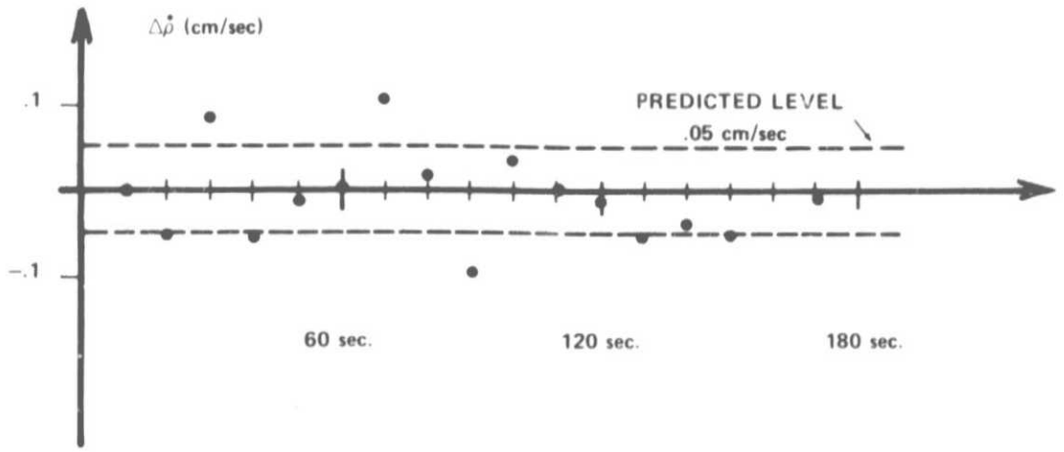

Figure 3. Tracking Systems Range-Rate Noise
Madrid → ATS-6 → Apollo/Soyuz → ATS-6 → Madrid

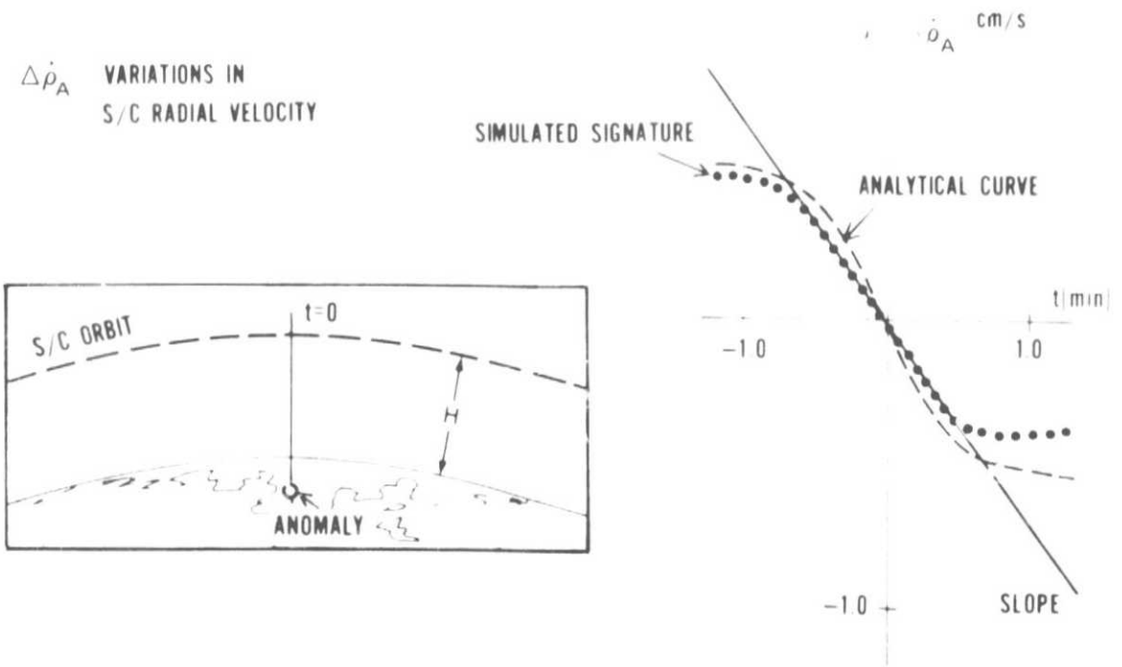

Figure 4. Analytical and Computer Simulated Signature for a 4° × 4°, 5 Mgal Anomaly

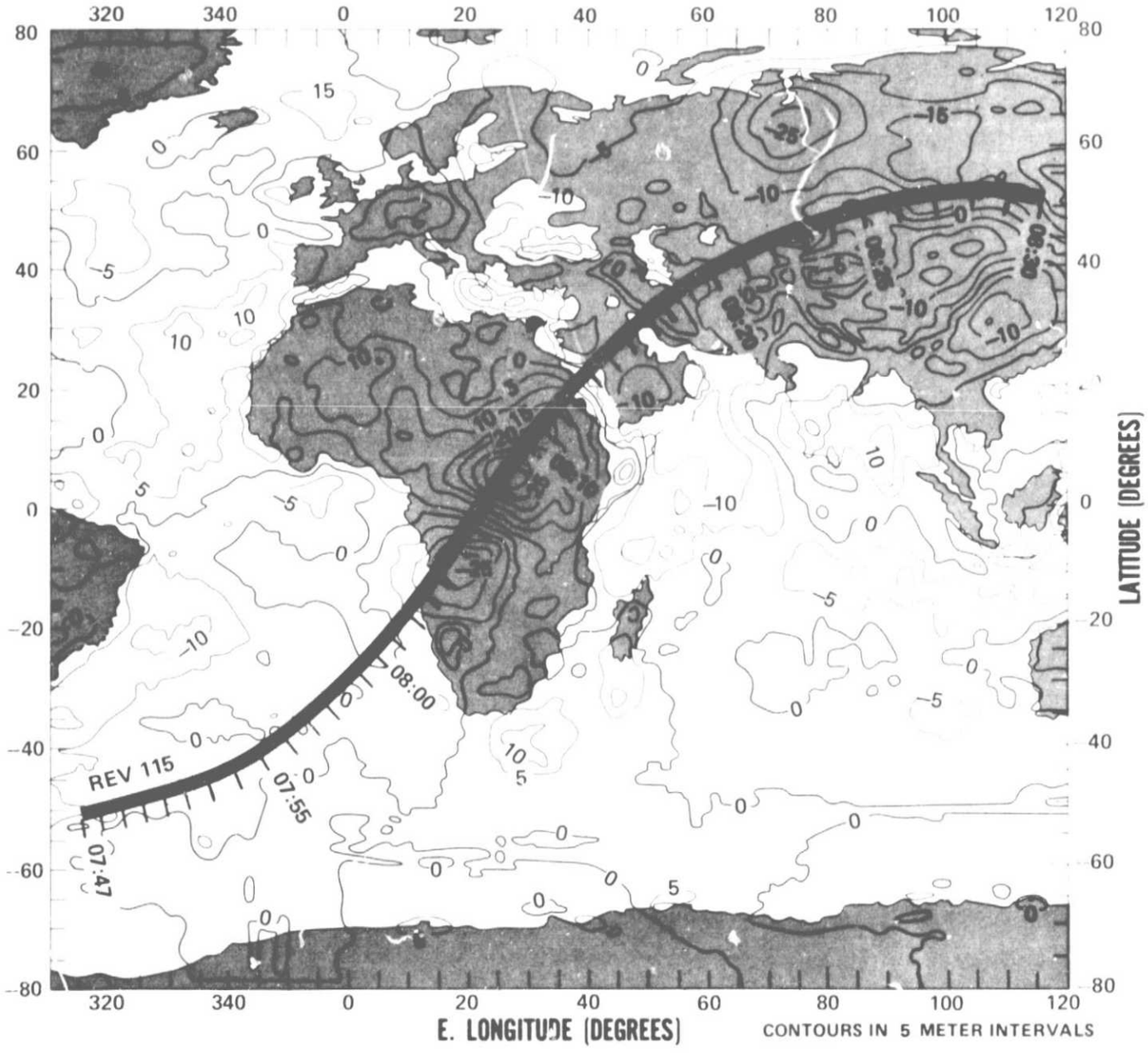

Figure 5. Residual Earth Surface Undulations (in m) (GEM-7 – GEM-8)

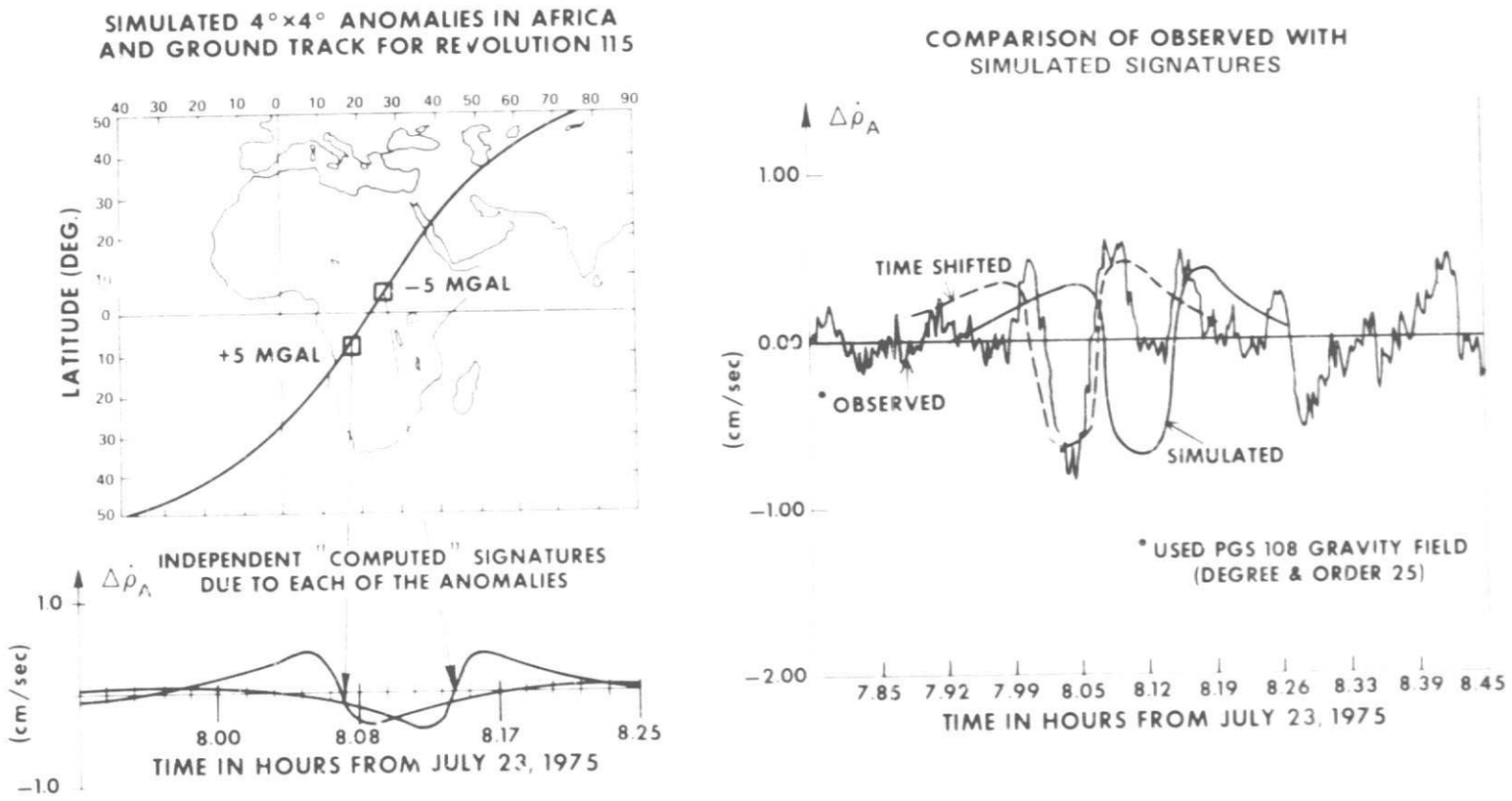

Figure 6. Ground Track for REV 115 used for 4° × 4° Anomaly Simulation in Africa

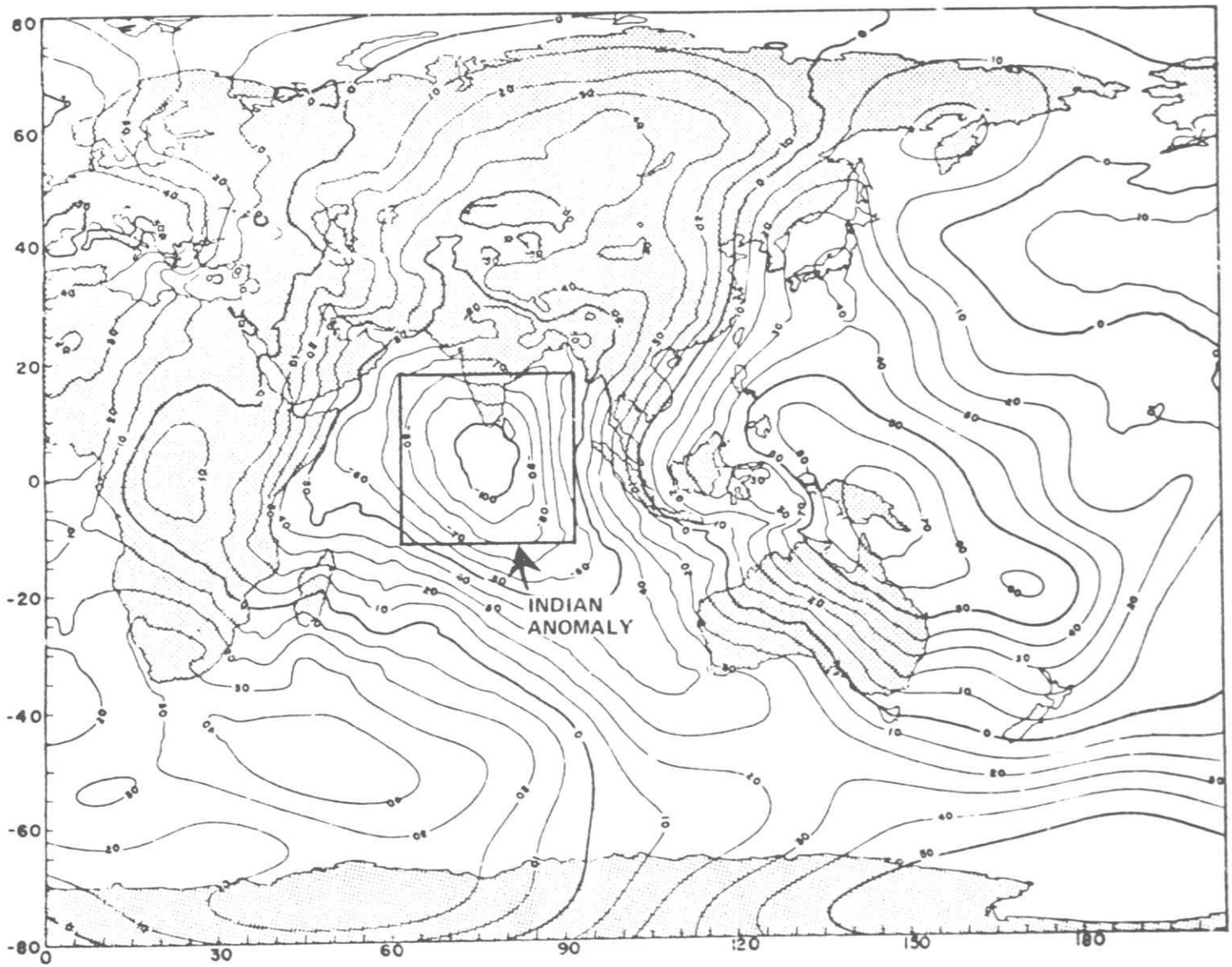

Figure 7. Global detailed gravimetric geoid, based upon a combination of the GSFC GEM-6 Earth Model and 1° × 1° surface gravity data.

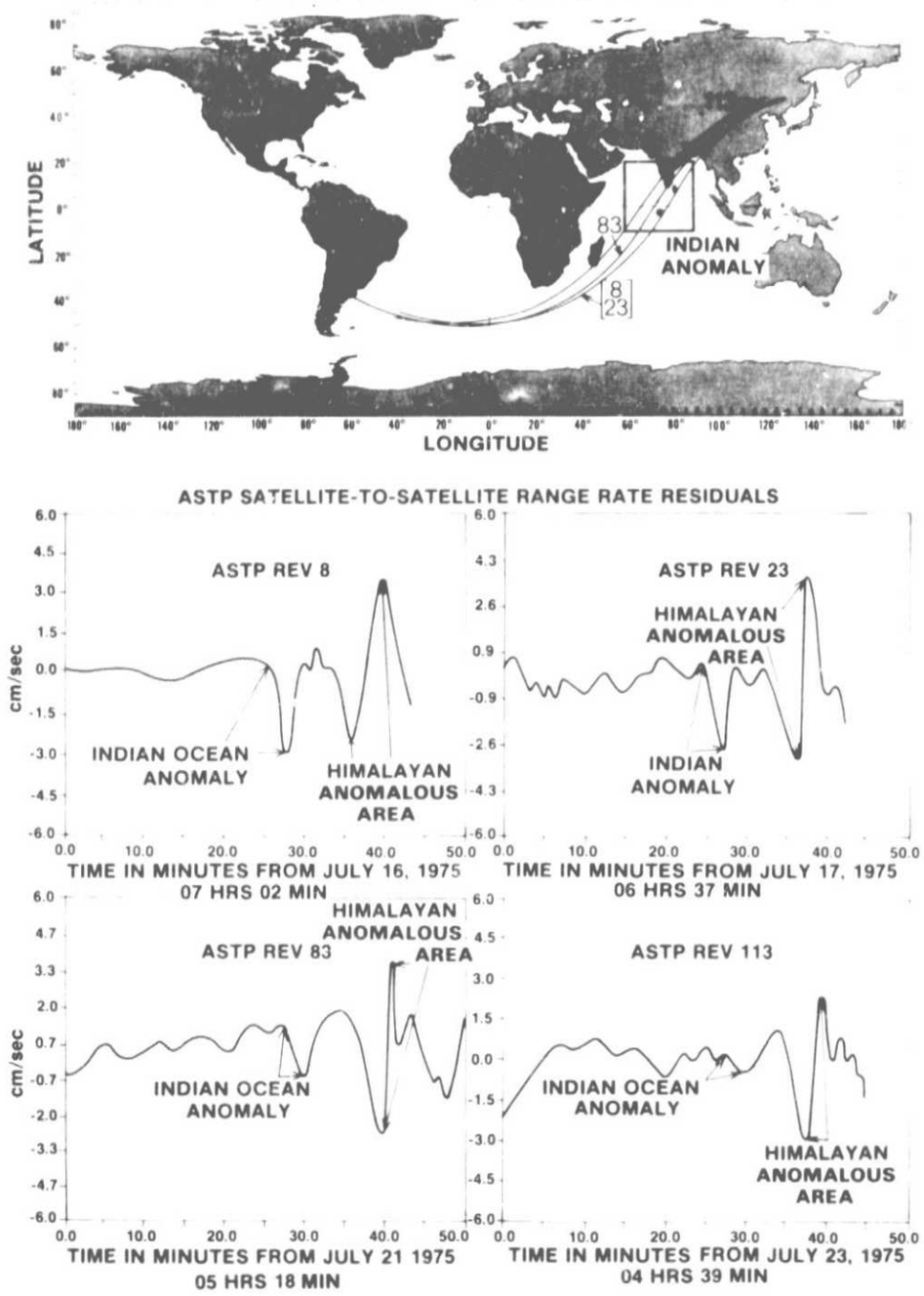

Figure 8. Range Rate Signatures of ASTP Revolutions in the Indian Ocean and Himalayan Areas.